A Retrofit 60 Hz Current Sensor for Power Monitoring at the Circuit Breaker Panel

John J. Cooley *Student Member, IEEE*, Daniel Vickery *Student Member, IEEE*, Al-Thaddeus Avestruz *Member, IEEE*, Zachary Clifford *Member, IEEE*, , and Steven B. Leeb *Fellow, IEEE*
Massachusetts Institute of Technology
Cambridge, MA 02139

***Abstract*—Improved signal conditioning electronics and new experimental results are presented for a sensor that measures current flow in a circuit breaker. A PIC microcontroller optimizes the phase reference for the synchronous detection system on startup eliminating the need for I/Q demodulation. Ultimately, the parts count of the signal conditioning electronics is halved compared to the previous work. Experimental results are presented demonstrating the sensor's response to 60 Hz signals with higher harmonic content and to step transients in 60 Hz signal amplitudes. The proposed current sensor does not require permanent modification of the breaker panel or the circuit breaker itself. The intent of this work is to develop a low-cost, non-intrusive, retrofit sensor for centralized power monitoring at the circuit breaker.**

I. Introduction and Motivation

Among the many potential benefits identified by the U.S. Department of Energy, the smart grid promises enormous energy savings through cost-effective demand-side energy management. Reducing the power consumed by utility costumers by just 5%, would "equate to permanently eliminating the fuel and greenhouse gas emissions from 53 million cars" [1]. The accessibility of power monitoring information will be a critical driver for the success of these efforts.

Centralized power monitoring systems promise lower sensor count than other "per-load sensor" systems. References [2]–[13] describe centralized power monitoring approaches in which loads are identified and then monitored according to their current signatures. Closed or "clamp" core sensors wrapped around the utility feed are often used to provide current sense signals. These sensors are impractical in many retrofit applications. For instance, skilled labor is required to separate line and neutral in order to deploy a wrap-around sensor, and in some industrial environments electrical service interruption may be intolerable or prohibitively expensive.

This paper proposes an alternative retrofit current sensor specifically aimed at widespread and accessible power monitoring. This sensor measures the current in the utility feed by sensing the resulting magnetic field at the face of the main (or other) circuit breaker in a standard breaker panel where the line and neutral are already separated. The sensor can be interrogated through the steel panel door with no direct electrical contact, permitting the door to remain closed to comply with safety regulations.

978-1-4244-7463-9/10/$26.00 @2010 IEEE

Previous work demonstrated preliminary results from a similar sensor [14]. This work presents improved signal conditioning electronics and new experimental results. A PIC microcontroller optimizes the phase reference for the synchronous detection system on startup eliminating the need for I/Q demodulation. Ultimately, the parts count of the signal conditioning electronics is halved compared to the previous work [14]. New experimental results are presented demonstrating the sensor's response to 60 Hz signals with higher harmonic content and to step transients in 60 Hz signal amplitudes.

II. System Overview

The sensor shown in Figure 1 consists of three parts: an inductive pickup for sensing current from the breaker face (Breaker Pickup), an inductive link designed to transmit power through the steel breaker panel door (Through-door Inductive Link), and a balanced JFET modulator circuit for transmitting information through the inductive link (Mixer).

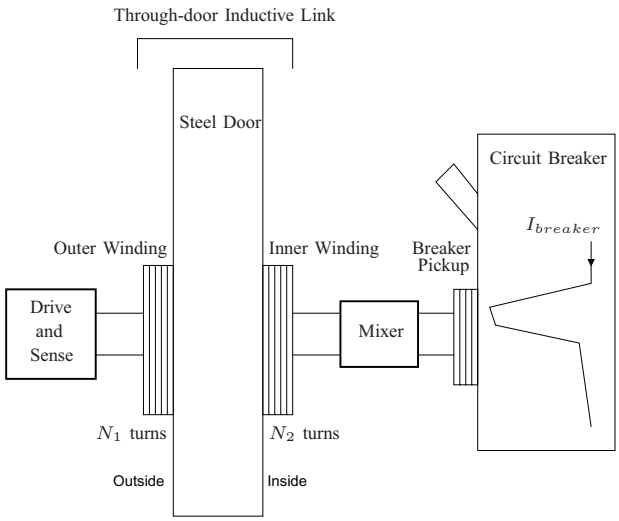

Fig. 1: System overview

The outer winding in Figure 1 is driven with a high-frequency sinusoidal carrier voltage. That voltage couples to the inner winding through the inductive link and drives the JFET mixer. The JFET mixer controls the amount of current

drawn from the inner winding according to the low-frequency (60 Hz) current signal measured by the breaker pickup. The result is a modulation between the high frequency carrier signal and the low-frequency (60 Hz) signal measured at the breaker face. The external sense circuit in Figure 1 monitors the current drawn through the inductive link to extract the resulting modulated signal. The JFET modulator is fully powered by the applied carrier, and the entire system works without modification to the breaker panel or the circuit breaker itself. With the modulated signal available to the sense circuit external to the door, the current through the main breaker may be analyzed with a centralized power monitoring system for load identification and diagnostics.

III. Breaker Pickup

This section describes the inductive sensor referred to as the "Breaker Pickup" in Figure 1. The current path inside a typical circuit breaker passes by the lower face as suggested by Figures 1 and 2. The breaker pickup, positioned outside the breaker on its lower face, was designed to focus and measure the resulting magnetic field.

Fig. 2: A cross-section of a typical circuit breaker.

To form the magnetic yoke for the breaker pickup, two halves of a high permeability core were joined for increased cross-sectional area. Several turns of magnet wire were wrapped around the yoke. A photograph of the breaker pickup affixed to the breaker face is shown in Figure 3. Maximizing the cross-sectional area and relative permeability of the core and the number of turns was important for increasing the inductance of the breaker pickup. The resulting inductive impedance at 60 Hz was sufficient to provide useable voltage signals corresponding to the breaker current.

IV. JFET Mixer

The four-quadrant balanced JFET mixer, shown in Figure 4, was designed to transmit information from the breaker pickup through the inductive link and out of the breaker panel. This circuit consists of two JFET devices for modulation control

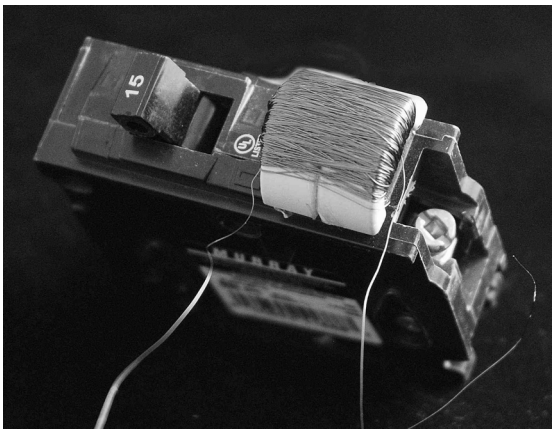

Fig. 3: A photograph of the breaker pickup.

and two resistors to improve linearity. The JFET mixer does not require a DC power supply. The two-JFET mixer circuit is particularly advantageous for this application because it requires a minimal amount of circuitry inside the breaker door and lends itself to a low-cost solution.

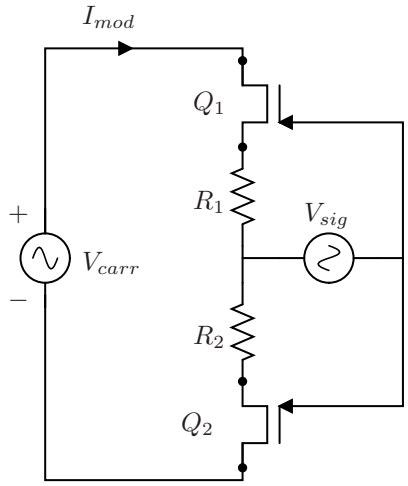

Fig. 4: Adaptive Referencing Balanced two-JFET Modulator circuit enables simultaneous powering and modulation with no DC bus.

In Figure 4, the JFET mixer may be modeled as a time-varying load on the carrier voltage source, $V_{carrier}$. The carrier voltage source corresponds to the voltage on the inner winding of the through-door link in Figure 1. The load presented to $V_{carrier}$ in Figure 4 varies with the control signal, V_{sig}, applied to the JFET gates leading to a modulation of the current I_{mod}.

The JFET is a normally-on device that requires a negative gate-to-source voltage, V_{gs}, to turn off. It may be modeled as a symmetric device, so that the drain and source are interchangeable. In general, the source may be identified as the leg of the JFET having the lower potential. On positive half cycles ($V_{carr} > 0$), the source of each device in Figure 4 is the lower leg and the drain, the upper leg. The gate-source voltage of the lower device is the positive-valued drain-source

voltage of the lower device added to the positive-valued drop across R_2 and V_{sig}. If the 60 Hz signal, V_{sig}, is sufficiently small, the lower device maintains a strictly positive gate-source voltage for most of the positive half cycle of the carrier signal. Thus the lower device can be taken to be fully on during that time, well-modeled by a small resistance. Meanwhile, the upper device has a gate-to-source voltage that is V_{sig} minus the positive drop across R_1. Again, if the 60 Hz signal, V_{sig}, is sufficiently small, the upper device maintains a gate-source voltage that *may not be* strictly positive so that its current is controlled according to the 60 Hz signal. In general, the gate-source voltage for the lower device contains a positive dc offset compared to that of the upper device even if they are not strictly positive and strictly negative respectively.

The roles of the two devices reverse when the polarity of the carrier signal reverses. The result is a modulation of the carrier signal current by the 60 Hz signal. The JFET mixer is adaptively-referencing because during both positive and negative half-cycles of $V_{carrier}$, one device is fully-on, referencing the source of the other device to the low-potential end of the mixer circuit.

The behavior described above can be validated by simulations (LTSPICE) of the circuit in Figure 4. Figure 5(a) shows simulations of the gate-to-source voltages for the upper and lower devices with a fixed positive carrier voltage. The gate-to-source voltage of the lower device contains a positive dc offset relative to that of the upper device. Figure 5(b) shows the resulting 60 Hz-modulated current when the circuit is excited with an ac-carrier voltage of 5kHz. Note that the quantities in the simulations of Figure 5 were chosen to provide illustrative visualizations of the behavior but do not necessarily correspond to design values or signal levels in our experimental setup. The plots of Figure 5 are also identical upon reversing the JFET devices with respect to the drain and source terminals, consistent with the drain-source symmetry of the JFETs described above.

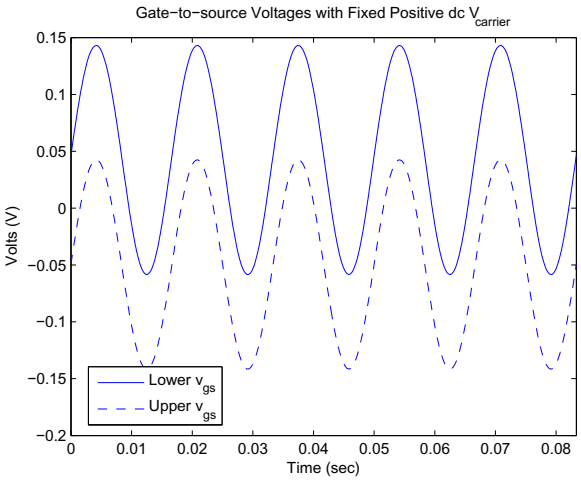

(a) Gate-to-source voltages with a fixed dc $V_{carrier} = 10V$.

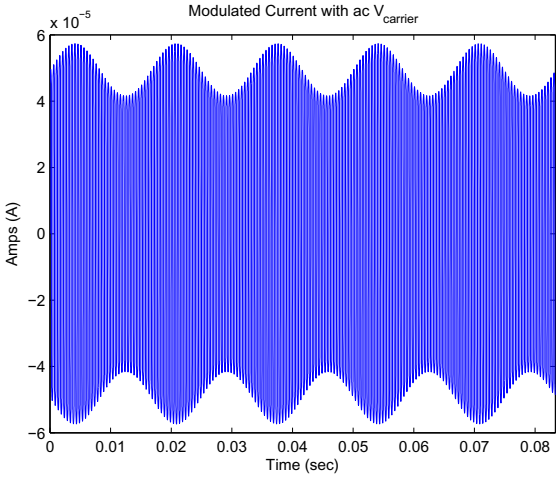

(b) Modulated current, I_{mod}, with a 2kHz 10V amplitude $V_{carrier}$.

Fig. 5: Balanced JFET Mixer, adaptive referencing and modulation behavior. PN4117 devices, $R_1 = R_2 = 1k\Omega$, $|V_{sig}| = 0.1$V, $f_{sig} = 60$Hz.

V. Through-door Inductive Link

The through-door inductive link in Figure 1 consists of two windings with a $\frac{N_2}{N_1}$ turns ratio. A large turns ratio was chosen to maximize voltage transfer to the inner winding and current transfer to the outer winding. The number of turns on the inner winding was upper-bound by space constraints. The number of turns on the outer winding was lower-bound by the current drive capability of the drive circuit producing the carrier signal.

We attempt to reduce the permeability of the steel using permanent magnets while providing a convenient means of securing the device to the door. The arrangement of the magnets shown in Figure 6 is intended to saturate the magnetic domains in the steel. The magnets are arranged so that the N and S poles of magnets on opposite sides of the door face each other.

A useful carrier frequency for the through-door inductive link was found empirically as follows. The demodulated 60 Hz signal at the final output of the system (See Section VI) was viewed on an oscilloscope while the carrier frequency was adjusted. For each adjustment of the carrier frequency, the value of the sense impedance used to measure the modulated current from the through-door link was also adjusted to maximize the demodulated signal. A suitable carrier frequency of approximately 220 kHz was identified for our experimental setup. This method of carrier frequency selection could be automated if the carrier frequency and primary side current sense impedance were electronically adjustable.

VI. Coil Drive and Signal Conditioning

The electronics on the outside of the breaker panel consist of two parts: 1) the carrier signal drive for the outer winding of the through-door link 2) the signal conditioning electronics for processing the modulated signal.

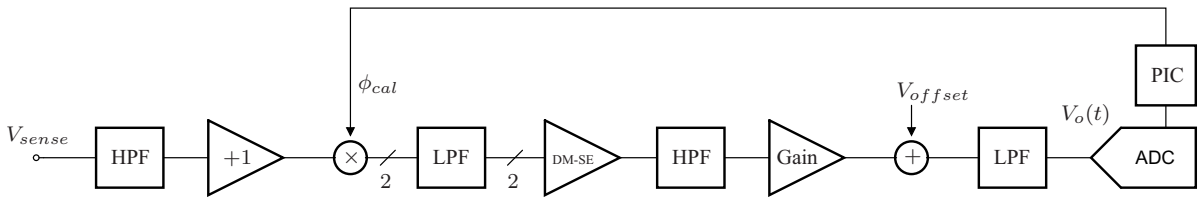

Fig. 8: A functional block diagram of the signal conditioning electronics

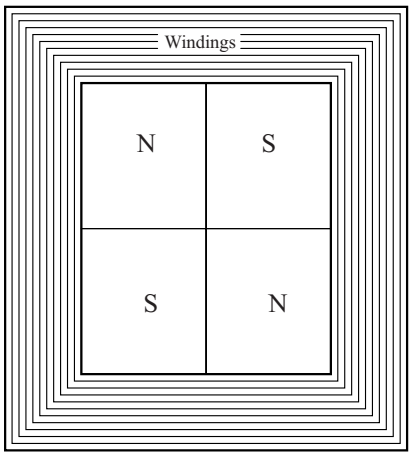

Fig. 6: Top view of transmission coil configuration

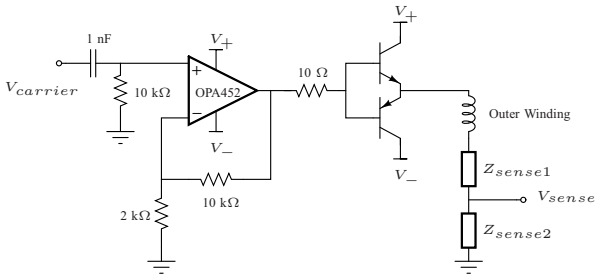

Fig. 7: A simplified schematic of the coil circuit.

A. Coil Drive

The coil drive circuit is shown in Figure 7. The carrier signal voltage is first high-pass filtered to reduce dc current in the outer winding. A high speed op-amp (OPA452) drives the bases of two BJT's in a push-pull configuration. The push-pull driver is connected to the series combination of the outer winding and two sense impedances. Splitting the sense impedance into two elements allows the designer to decouple the signal conditioning input amplitude constraint from other considerations, e.g. impedance matching between the outer winding and the total sense impedance.

B. Signal Conditioning

A functional block diagram of the signal conditioning system is shown in Figure 8. The voltage, V_{sense} from Figure 7, is taken as the input signal to the signal conditioning electronics in Figure 8. A high-pass filter first strips any dc from the input signal in order to minimize unwanted harmonic content in the demodulated output from the ensuing multiplier. The signal is then buffered and multiplied with a phase-controlled carrier reference (see Section VI-B1). Demodulation is achieved with a differential-mode output square wave multiplier. The multiplier is implemented using a full-bridge of analog switches. A fully-differential low-pass filter attenuates high-frequency residue left after demodulation and a differential-mode to single-ended converter (DM-SE) ground-references the resulting signal. A high-pass filter strips the dc content left from demodulation of the unsuppressed carrier in V_{sense}. Finally, the signal is gained. An offset voltage, V_{offset}, and an anti-aliasing low-pass filter accommodate the ensuing analog-digital converter (ADC).

Perhaps the primary limitation of this signal conditioning approach originates in the treatment of the unsuppressed carrier content in V_{sense}. The dc content resulting from demodulation of that carrier limits the gain that can be applied to the signal. Because the gain must be applied late in the signal chain (after the HPF), accumulated noise from the electronics upstream of that stage limits the SNR of the demodulated output signal. Nonetheless, Section VII will show useful resolution of current signals in the circuit breaker. Further work may investigate other topologies for addressing the unsuppressed carrier content earlier in the signal chain.

1) Phase Calibration: The PIC in Figure 8 generates carrier frequency signals to control both the coil drive and the demodulator. To account for the phase shift in the signal path between the coil drive and the demodulator, the phase of the multiplier control signal with respect to that of the coil drive is automatically calibrated upon system initiation. The calibration process uses a hill-climbing algorithm designed to minimize the amplitude of the demodulated signals at the output. The hill-climbing algorithm, embedded in the PIC of Figure 8, is illustrated by the flow diagram in Figure 9.

Assuming high frequency terms from the demodulator have been perfectly eliminated by the ensuing low-pass filter, and any dc terms from the down-modulated carrier have been eliminated by the high-pass filter, the final demodulated output signal can be shown to be:

$$V_o(t) = cos(-\phi)\left(\frac{M}{2}cos(\omega_m t)\right) \tag{1}$$

where $M/2$ is the amplitude of the modulated signal, ω_m is the modulation frequency, and ϕ is the undetermined phase offset that we wish to calibrate. This phase offset is unknown because it depends on the properties of the breaker panel door

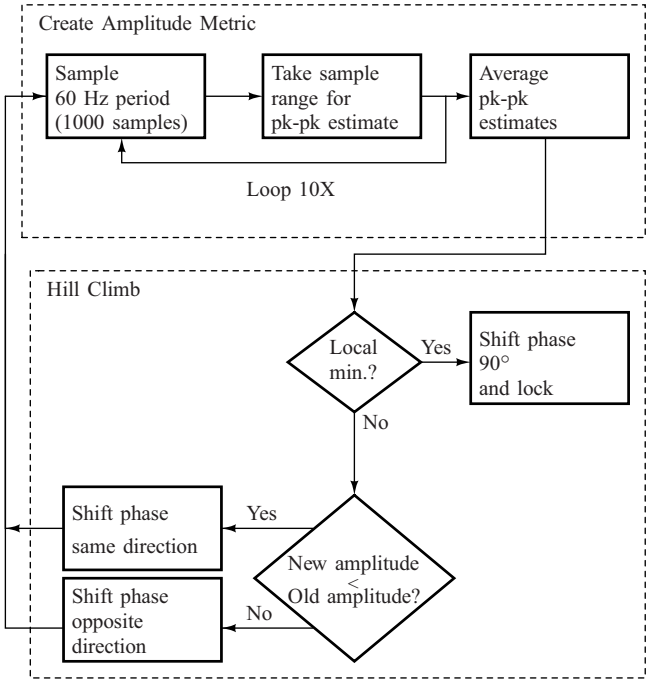

Fig. 9: A flowchart of the phase calibration algorithm.

in addition to the properties of the through-door link and the modulator circuit.

The algorithm first minimizes the $cos(-\phi)$ term in (1) by incrementally shifting the phase of the mixer reference signal. The phase is shifted in the direction of decreasing amplitude of the demodulated signal, thus "hill-climbing" toward the global minimum. Once this minimum is reached, the phase of the mixer reference signal is shifted by 90°, maximizing the $cos(-\phi)$ term and the amplitude of the demodulated signal. Note that this algorithm does not suffer from the problem of local minima, because our heuristic of signal amplitude is convex, such that the only local minimum is also the global minimum.

The amplitude metric used in calibration is generated from peak-to-peak measurements averaged over several 60 Hz periods. Arrival at the minimum can be detected by a simple threshold in the case of a known test current, or failure to leave a small phase range within a limited number of hill-climbing iterations.

Once the optimum phase has been determined, the PIC stores the corresponding value in memory and "opens the loop" to avoid washing out the signal of interest during runtime. Further work may investigate feedback loop bandlimiting approaches to allow for slow closed-loop phase tracking during runtime.

VII. Experimental Setup and Results

Photographs of the experimental setup are shown in Figure 10. An HP 6834B ac power source was used to generate sinusoidal test current signals, and a Bestec ATX-300-12E computer power supply was used to generate a non-sinusoidal

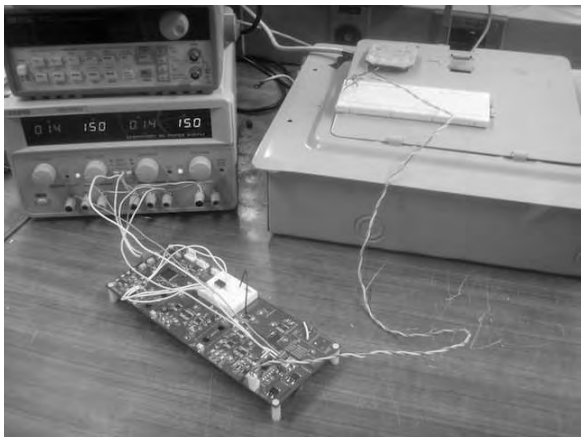

(a) The experimental setup with the panel door closed.

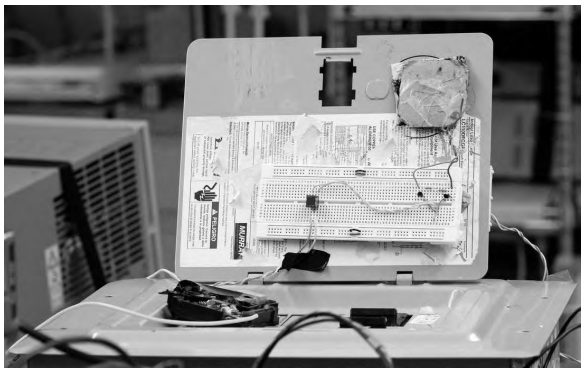

(b) The experimental setup with the panel door open.

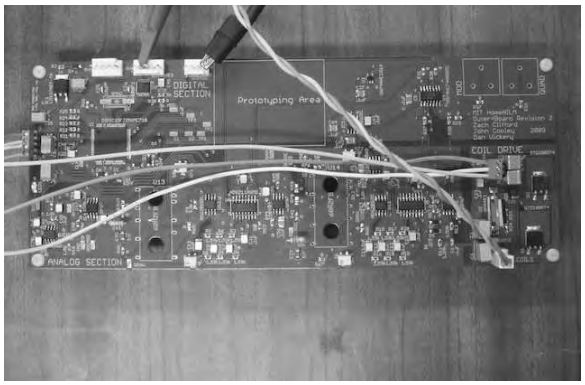

(c) The PCB with the drive and signal conditioning electronics.

Fig. 10: Photos of the experimental setup.

test current typical of AC-DC converters. The breaker pickup core was constructed with two halves of a toroidal high-permeability core ($\mu = 10,000$) joined together and secured to the breaker face. The mixer was attached to the inside surface of the steel door. An audio-frequency transformer (Tamura MET-01) was inserted between the breaker pickup leads and the modulation input leads to the mixer for for better modulation. This portion of the experimental setup is shown in Figure 10(b). The inner winding consisted of 1000 turns of 34 AWG magnet wire and the outer winding consisted of 24 turns. Both windings were wrapped directly around four

samarium cobalt magnets of dimension 1/2”x1/2”x1/4” and grade 26 MGOe as described in Section V. The mixer in Figure 4 was built from two PN4117A JFET devices (Fairchild semiconductor), and two 1.2 kΩ resistors.

Experimental results from the prototype monitoring hardware are shown in Figures 11-13. The HP 6834B ac source was used to provide different frequencies and amplitudes of current through the test circuit breaker monitored by the prototype sensor. The programmable ac source made it possible to simulate step transients between amplitudes as well. The sample ATX power supply produced current waveforms with higher harmonic content. The harmonic content of the ATX supply current is typical for an unfiltered or lightly filtered full-bridge rectifier at the front-end of many AC-DC power supplies.

Figure 11 shows the performance of the current sensor for a simple 60 Hz sinusoidal current flowing through the breaker. Figures 11(a) and 11(c) depict the input test current as measured across a 2 Ω load and the reconstructed or demodulated output. Figure 11(b) shows a spectrum analyzer screen capture of the modulated carrier on the primary side or “outside” the door of the circuit breaker panel. As expected, the spectrum shows a strong peak at the carrier frequency. The side-lobes correspond to the modulating current signal at 60 Hz differences from the carrier frequency.

Figure 12 shows a measurement of an amplitude step transient in a 60 Hz sinusoidal signal generated by the HP 6834B source. In the plot, the green or lighter trace represents the input current from the source, and the pink or darker trace is the reconstructed signal.

Figure 13(a) shows the time-domain reconstruction of a non-sinusoidal signal produced by an ATX power supply. The top trace in Figure 13(a) represents the current drawn by the ATX power supply, and the bottom trace shows the reconstructed signal. Band-limiting in the signal chain at about 1 kHz limits the accuracy of the reconstruction. To verify this further, the DTFTs of the input and output current waveforms were calculated using the FFT in MATLAB®. The results are shown in Figure 13(b). Extending the bandwidth of the system or extracting an inverse filter should enable improved harmonic reconstruction.

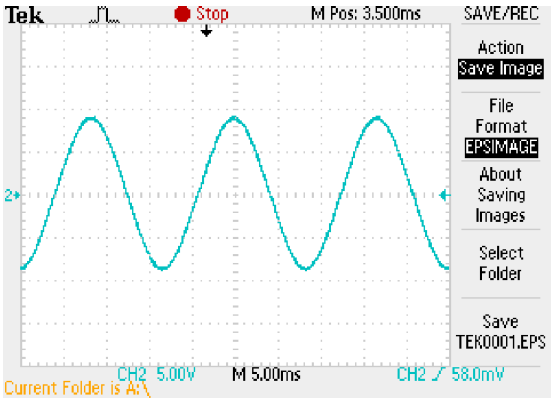

(a) Time-domain 4.5 A (peak) input current

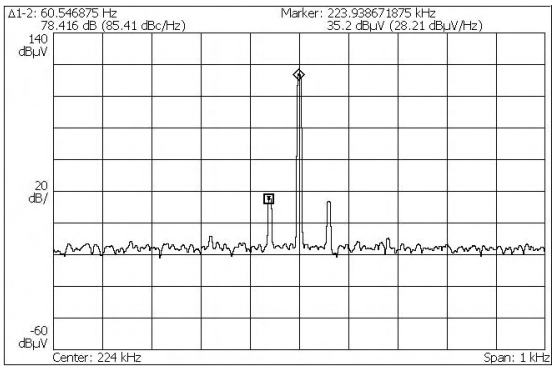

(b) Frequency-domain upmodulated signal

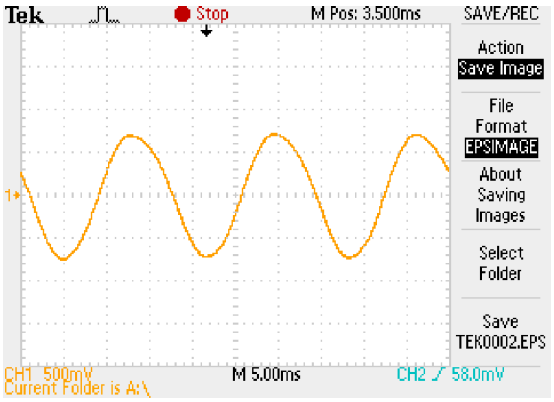

(c) Time-domain demodulated output

Fig. 11: 60 Hz sinusoidal current

VIII. Conclusion

The U.S. Department of Energy has identified “sensing and measurement” as one of the “five fundamental technologies” essential for driving the creation of a “Smart Grid” [1]. Consumers will need “simple, accessible. . . , rich, useful information” to help manage their electrical consumption without interference in their lives [1]. Both vendors and consumers will likely find innumerable ways to mine information if it is made available in a useful form. However, appropriate sensing and information delivery systems remain a chief bottleneck for many applications, and metering hardware and access to metered information will likely limit the implementation of new electric energy conservation strategies in the near future.

This paper proposes an alternative to traditional clamp or Hall-effect sensors. This alternative requires no skilled installation. This sensor measures the current in the utility feed by sensing the resulting magnetic field at the face of the main (or other) circuit breaker in a standard breaker panel. The sensor can be interrogated through the steel panel door with no direct electrical contact, permitting the door to remain closed to comply with safety regulations.

The proposed sensor could be a “silver bullet” for many power monitoring and control problems. The sensor is as easy to install in a retrofit situation as in new work. This approach could make it easy to provide essential, comprehensible in-

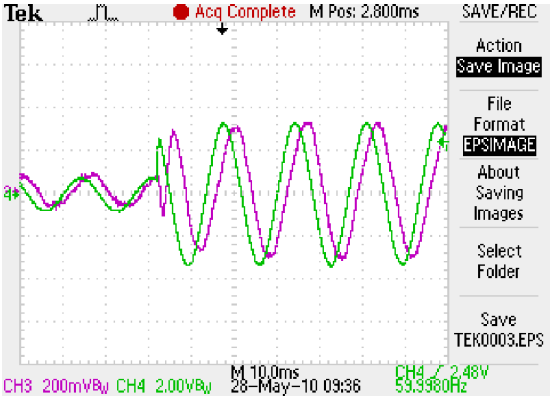

Fig. 12: 60 Hz sinusoidal current with an amplitude step transient from 500 mA to 2 A (peak).

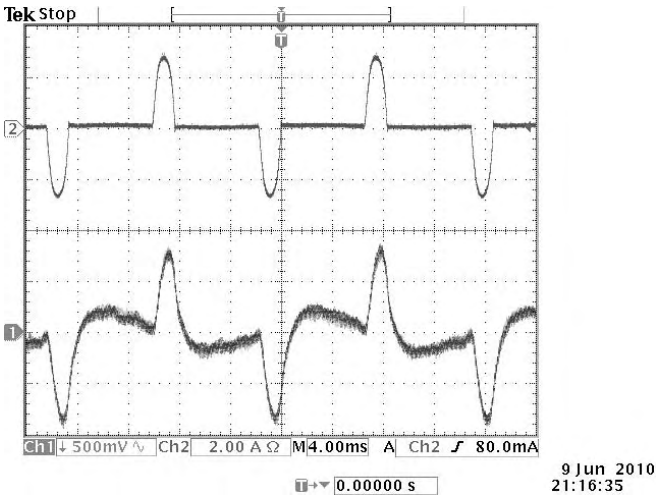

(a) Time-domain: Input (top), Output (bottom)

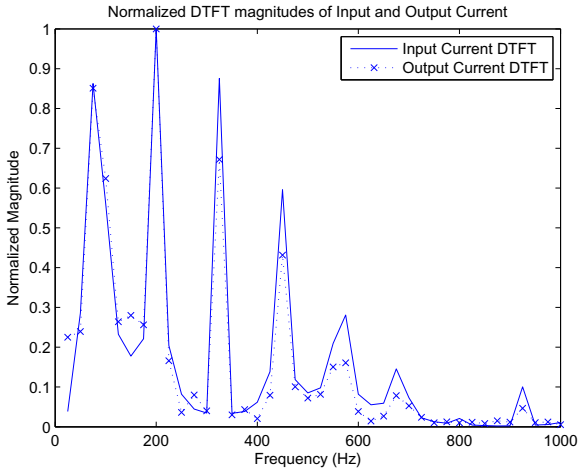

(b) Frequency-domain

Fig. 13: Non-sinusoidal test current from ATX AC-DC power supply.

formation about opportunities and the success of efforts for energy conservation.

Acknowledgment

The authors would like to thank The Grainger Foundation and BP-MIT research alliance for their generous and necessary support and funding. This work was partially supported by the Center for Materials Science and Engineering at MIT as part of the MRSEC Program of the National Science Foundation under grant number DMR-08-19762.

References

[1] U. S. D. of Energy, "The smart grid: An introduction," August 2009. [Online]. Available: http://www.oe.energy.gov/1165.htm

[2] J. S. Ramsey, S. B. Leeb, T. DeNucci, J. Paris, M. Obar, R. Cox, C. Laughman, and T. J. McCoy, "Shipboard applications of non-intrusive load monitoring," in *American Society of Naval Engineers Reconfigurability and Survivability Symposium*, Atlantic Beach, Florida, February 2005.

[3] T. DeNucci, R. Cox, S. B. Leeb, J. Paris, T. J. McCoy, C. Laughman, and W. Greene, "Diagnostic indicators for shipboard systems using non-intrusive load monitoring," in *IEEE Electric Ship Technologies Symposium*, Philadelphia, Pennsylvania, July 2005.

[4] W. Greene, J. S. Ramsey, S. B. Leeb, T. DeNucci, J. Paris, M. Obar, R. Cox, C. Laughman, and T. J. McCoy, "Non-intrusive monitoring for condition-based maintenance," in *American Society of Naval Engineers Reconfigurability and Survivability Symposium*, Atlantic Beach, Florida, February 2005.

[5] S. B. Leeb, S. R. Shaw, and J. J. L. Kirtley, "Transient event detection in spectral envelope estimates for nonintrusive load monitoring," *IEEE Transactions on Power Delivery*, vol. 10, no. 3, pp. 1200–1210, July 1995.

[6] L. K. Norford and S. B. Leeb, "Non-intrusive electrical load monitoring in commercial buildings based on steady state and transient load-detection algorithms," *Energy and Buildings*, vol. 24, pp. 51–64, 1996.

[7] U. A. Khan, S. B. Leeb, and M. C. Lee, "A multiprocessor for transient event detection," *IEEE Transactions on Power Delivery*, vol. 12, no. 1, pp. 51–60, 1997.

[8] S. R. Shaw, S. B. Leeb, L. K. Norford, and R. W. Cox, "Nonintrusive load monitoring and diagnostics in power systems," *IEEE Transactions on Instrumentation and Measurement*, vol. 57, no. 7, pp. 1445–1454, July 2008.

[9] G. R. Mitchell, R. W. Cox, J. Paris, and S. B. Leeb, "Shipboard fluid system diagnostic indicators using non-intrusive load," *Naval Engineers Journal*, vol. 119, no. 1, November 2007.

[10] J. P. Mosman, R. W. Cox, D. McKay, S. B. Leeb, and T. McCoy, "Diagnostic indicators for shipboard cycling systems using non-intrusive load monitoring," in *American Society for Naval Engineers Day 2006*, Arlington, VA, June 2006.

[11] R. W. Cox, P. Bennett, D. McKay, J. Paris, and S. B. Leeb, "Using the non-intrusive load monitor for shipboard supervisory control," in *IEEE Electric Ship Technologies Symposium*, Arlington, VA, May 2007.

[12] G. Mitchell, R. W. Cox, M. Piber, P. Bennett, J. Paris, W. Wichakool, and S. B. Leeb, "Shipboard fluid system diagnostic indicators using nonintrusive load monitoring," in *American Society for Naval Engineers Day 2007*, Arlington, VA, June 2007.

[13] E. Proper, R. W. Cox, S. B. Leeb, K. Douglas, J. Paris, W. Wichakool, L. Foulks, R. Jones, P. Branch, A. Fuller, J. Leghorn, and G. Elkins, "Field demonstration of a real-time non-intrusive monitoring system for condition-based maintenance," in *Electric Ship Design Symposium*, National Harbor, Maryland, February 2009.

[14] Z. Clifford, J. Cooley, A.-T. Avestruz, Z. Remscrim, V. Dan, and S. Leeb, "A retrofit 60 hz current sensor for non-intrusive power monitoring at the circuit breaker," in *Applied Power Electronics Conference and Exposition (APEC), 2010 Twenty-Fifth Annual IEEE*, 21-25 2010, pp. 444 –451.